JOURNAL OF MATERIALS SCIENCE **38** (2003) 1413– 1423

Characterisation of $Ce_{0.8}Gd_{0.2}O_{1.9}$/3Y-TZP composite electrolytes—effects of weight % 3Y-TZP particles

R. J. BALL*, R. STEVENS
Department of Engineering and Applied Science, University of Bath, Bath, BA2 7AY, UK
E-mail: Richard.Ball@bristol.ac.uk
E-mail: R.Stevens@bath.ac.uk

Solid oxide fuel cell electrolytes are currently manufactured from zirconia. This is due to its high ionic conductivity and mechanical strength. However, a disadvantage of zirconia is the high temperatures required for efficient operation, greater than 900°C for cells not utilising thin supported electrolytes. A study to characterise the properties of an alternative composite solid electrolyte, based on a gadolinia doped ceria matrix surrounding yttria stabilised tetragonal zirconia particles is presented. Composite samples produced using 1, 2, 5, 10 and 20 wt% zirconia particles were characterised using a range of different experimental techniques including scanning electron microscopy, transmission electron microscopy, X-ray diffraction, mechanical testing and impedance spectroscopy. Results showed a lowering in flexure strength of the experimental composite samples with the addition of particles. It is considered that the particles acted as regions where cracks could initiate. © *2003 Kluwer Academic Publishers*

1. Introduction

Fuel cells are a promising source of energy for future generations in terms of reduced environmental impact compared to other alternatives such as gas-fired power stations. Currently, solid oxide fuel cells (SOFC's) with efficiencies greater than 60% for single systems and 85% for combined heat and power have been manufactured and used for commercial operation [1].

A fuel cell is constructed from a number of principle parts including the electrolyte, anode, cathode, interconnect and auxiliary components. Commercial SOFC's utilise a thin (<10 μm), high density, yttria stabilised zirconia (YSZ) layer as the solid electrolyte [2–4]. Zirconia is appropriate due to its high oxygen ion conductivity, low electronic conductivity and good mechanical properties. However, a disadvantage associated with the use of zirconia is that the desired properties are only available at high operating temperatures in excess of 900°C, unless thin supported electrolyte designs are utilised. This not only reduces the efficiency, but also requires auxiliary components to be made from materials that can withstand these temperatures. This adds significantly to the SOFC's total manufacturing cost. In addition high operating temperatures can lead to sealing problems between cell components, especially during the initial heating, if coefficients of thermal expansion are not suitably matched.

Replacement of the electrolyte with an alternative material, which does not require the high operating temperatures of zirconia, could increase efficiency and reduce the overall manufacturing cost significantly. A promising candidate as a replacement is doped ceria [5–7]. Ceria can be alloyed with a number of aliovalent transition and rare earth ions to produce ionically conducting ceramics. Previous research has identified gadolinium oxide as a particularly appropriate addition due to the high ionic conductivities achievable. Gadolinia doped ceria has a significantly higher oxygen ion conductivity compared to zirconia, at a reduced temperature, making it ideal for use in low and intermediate temperature fuel cells. However there are a number of problems associated with the use of this ceramic.

During operation, degradation of the electrolyte caused by reduction of ceria from Ce^{4+} to Ce^{3+} can occur on the anode side of the electrolyte. This results in an increased level of electronic conductivity and lattice expansion. Electronic conductivity leads to internal short-circuiting caused by electron leakage between the anode and cathode across the electrolyte, and lattice expansion contributes to mechanical stresses. The severity of these problems can be decreased by reducing the operating temperature to around 500°C. This reduces the electronic contribution of the conductivity to a level where the overall cell performance is not significantly affected [8, 9]. If a slightly higher operating temperature is desired, a thin layer of zirconia can be applied to the electrolyte, acting as an insulator to electron flow without significantly effecting the ionic conductivity.

Present Address: Interface Analysis Centre, University of Bristol, Bristol BS2 8BS, UK, e-mail: Richard.Ball@bristol.ac.uk.

In addition to the electrical problems associated with ceria, its mechanical properties are significantly inferior to those of zirconia, with the room temperature strength of zirconia and doped ceria being 1000 MPa [10] and 140–180 MPa [11, 12] respectively. The higher mechanical strength exhibited by zirconia can be explained by the transformation toughening mechanism.

Zirconia is most stable in its cubic form, however it can be partially stabilised in the tetragonal structure by the addition of small amounts, 3–12 wt%, of stabilising oxides such as yttria (Y^{3+} ion). When the tetragonal zirconia is subjected to an increased tensile stress, such as that present around the tip of a propagating crack, the tetragonal to monoclinic phase transformation occurs. This phase transformation is associated with a 4% increase in volume resulting in the crack tip being put into compression and the rate of crack propagation being reduced.

A common method used to improve the mechanical properties of ceramic materials is the addition of tetragonal zirconia particles thus introducing the transformation toughening mechanism. However, previous research by the authors suggests that when this approach is used in doped ceria a significant increase in the activation energy for ionic conduction occurs. This was attributed to the formation of a solid solution [13].

In this paper the effects of adding agglomerates of tetragonal zirconia particles, to a gadolinia doped ceria matrix, is investigated. It is envisaged that the reduced surface area associated with larger particles will limit the diffusion of zirconia ions into the ceria matrix thereby decreasing the formation of solid solution and associated reduced conductivity. A number of composite samples were manufactured consisting of zirconia particles surrounded by a gadolinium doped ceria matrix. Different weight fractions of YSZ particles were added in the range of 1 and 20%.

2. Experimental methods

2.1. Fabrication of ceramic samples

All samples were produced using a 20% gadolinia doped ceria ($Ce_{0.8}Gd_{0.2}O_{1.9}$) matrix, manufactured by Rhodia, surrounding particles of 3 wt% YSZ powder, manufactured by Daichii. Zirconia particles were produced by spray drying, prior to calcining at 1300°C for a duration of 4 hours. 1, 2, 5, 10 and 20 wt% calcined zirconia particles were then added to gadolinia doped ceria and mixed in ethanol using a ball mill for 1 hour. Only a small amount of zirconia grinding media was added to the milling vessel. This allowed mixing of the powder without the tumbling action of the balls breaking the zirconia particles and smaller agglomerates. Mixed powders were dried under a heat lamp, sieved and then pressed into 15 mm diameter tablets using a cylindrical die. 1 g of powder was used in the manufacture of each tablet, resulting in a sample thickness of approximately 1.1 mm. Samples were cold isostatically pressed at 150 MPa for 90 seconds prior to sintering. Sintering was carried out at 1500°C for a duration of 4 hours. Ramp rates of 3°C min^{-1} were used.

2.2. Porosity measurements

The porosity of sintered ceramic samples was determined using a mercury displacement method. This involved measuring the sample weight, m, and the, upthrust, u, produced by the sample when submerged in a denser medium of mercury. True sample volume, not including pores, was calculated from the sample weight and theoretical density of the ceramic, ρ_s, obtained from crystallographic data, using Equation 1. A density value of 7.295 g cm^{-3} was used for $Ce_{0.8}Gd_{0.2}O_{1.9}$ and 5.83 g cm^{-3} for 3Y-TZP. The total sample volume, including pores, was obtained from the sample upthrust when submerged in mercury, and density of mercury, ρ_{Hg}, using Equation 2. This can be done since mercury is unable to fill the pores of the ceramic sample due to its high surface tension and contact angle with ceramics. Percentage porosity is finally calculated using Equation 3, from the sample volumes, including and, not including pores.

$$\nu = \frac{m}{\rho_s} \tag{1}$$

$$\nu_p = \frac{u}{\rho_{Hg}} \tag{2}$$

$$\%\,\text{Porosity} = \frac{\nu_p - \nu}{\nu_p} \cdot 100\% \tag{3}$$

2.3. Determination of modulus of rupture

The modulus of rupture of each composite sample manufactured was determined by fracturing circular disks in the ball and ring test configuration. A slight variation in surface morphology of samples was observed and for this reason all samples were polished to a 3 micron diamond finish to ensure consistency of results. 10 samples were tested for each composite. An Instron 1122 universal testing machine was used to apply a compressive load to the ball and ring jig, thus fracturing samples. A load cell with a maximum full range deflection of 500 kg was used to measure loads, however the full range deflection was reduced wherever possible to reduce errors. The load and crosshead displacement was recorded using a chart recorder. All tests were carried out in accordance with the standard test method for ceramic substrates [14]. Flexure strength, σ_{max}, was calculated from the failure load, F, Poisson's ratio, ν, specimen thickness, t, specimen radius, R, support ring radius, a, and radius of the section under maximum stress, b, using Equation 4. An approximation of $b = t/3$ can be made since t is much greater than the contact radius with the sample surface.

$$\sigma_{max} = \frac{3F(1+\nu)}{4\pi t^2}\left[\frac{(1-\nu)(2a^2-b^2)}{(1+\nu)2R^2} + 2\ln\left(\frac{a}{b}\right) + 1\right] \tag{4}$$

2.4. Impedance spectroscopy

Impedance spectroscopy is essentially a non-destructive technique that can provide information that

cannot be obtained by other means. It is particularly useful for the study of mobile charges in ionic, semi-conducting or insulating solids [15]. This is due to its ability to resolve the individual contributions of impedance, from the grain boundary, grain interior and electrode of a sample. SOFC electrolytes are oxygen ion conductors and can therefore be studied using impedance spectroscopy. The use of impedance spectroscopy to determine the ionic conductivity of zirconia ceramics was first introduced by Bauerle in 1969 [16].

Impedance spectroscopy was used to characterise the electrical properties of the composite electrolytes. The frequency response of the composite materials, between 10^{-1} and 10^{7} Hz, was monitored using a Solartron 1260 Gain Phase Analyser. 20 readings per decade on a logarithmic scale were taken using a DC potential of 0V and AC amplitude of 1000 mV. Complex plane plots, real impedance Z′ versus imaginary impedance Z″, were constructed from the raw data using Solartron software 'Z-plot'. Values for the sample resistance were obtained using the circle fitting option on Z-plot. This facility allows a circle of best fit, corresponding to the characteristic semicircle produced by the frequency response of the sample, to be drawn on the complex plane plot. The diameter of such a circle is directly proportional to the sample resistance, thus allowing this value to be estimated. Previously measured sample dimensions were subsequently used to calculate the sample conductivity from the resistance using Equation 5, where, r, equals resistance, t, equals thickness and, a, equals the electrode area.

$$\sigma = \frac{t}{RA} \tag{5}$$

Impedance measurements for each sample were repeated every 50°C in the temperature range of 500 to 750°C. The measurements of sample conductivity at each temperature were then used to obtain a value for the activation energy for ionic conduction using Equation 6 [17, 18].

$$\sigma T = A_\sigma \exp\left[\frac{-\Delta H_\sigma}{RT}\right] = A_\sigma \exp\left[\frac{-\Delta E_\sigma}{kT}\right] \tag{6}$$

Equation 6 relates the sample conductivity, σ, at temperature, T, to the process enthalpy, ΔH_σ (J), or energy, ΔE_σ (eV). A_σ is a pre-exponential factor which contains several terms including the number of mobile ions involved in the conduction process.

2.5. Scanning electron microscopy

Fracture surfaces, produced during biaxial fracture strength measurements, were examined in a Jeol 6310 scanning electron microscope (SEM). Compositions containing a range of weight fractions of zirconia particles were examined. An Edwards sputter coater was used to deposit a thin layer of gold on the surface of each sample in order to prevent charging.

2.6. X-ray diffraction

Sintered samples were analysed using X-ray diffraction. A Phillips PW1730/00 X-ray diffractometer, emitting copper K_α radiation, was used to produce diffraction patterns in the 2-theta range of 25–65 degrees. Samples were scanned at a rate of 0.5 seconds per step with a step size of 0.02 degrees.

2.7. Transmission electron microscopy

The ceria/gadolinia composite containing 5% zirconia particles was examined using transmission electron microscopy (TEM). Samples were prepared in the form of 3 mm diameter disks that were dimpled in each side prior to ion beam thinning.

3. Results and discussion

The conductivity of the composite samples was determined using impedance spectroscopy. Impedance data is presented in the form of complex plane plots, real impedance, Z', versus imaginary impedance, Z''. An idealised complex plane plot for a ceramic material is shown in Fig. 1 with its corresponding equivalent electrical circuit. The diagram consists of a number of semicircles along the real impedance axis, each representing the grain interior, grain boundary, and electrode resistances respectively. Complex plane plots obtained for the composite samples, Fig. 2a–d contain only one semicircle, followed by a line of positive gradient at approximately 45 degrees. This indicates that the contributions of the sample resistance from the grain interior and grain boundary cannot be resolved. This is a likely consequence of the relatively high temperatures employed, the measurements having been taken at, 500–750°C. Fig. 2e shows a labelled complex plane plot. As no useful data can be extracted from the frequency response of the electrode a number of readings were taken over a reduced frequency range. This increased the clarity of the figures without compromising the data contained within them. It should be noted that the size of the semicircles decrease with increasing temperature.

Plots of conductivity versus composition for the samples at each temperature between 500 and 750°C is

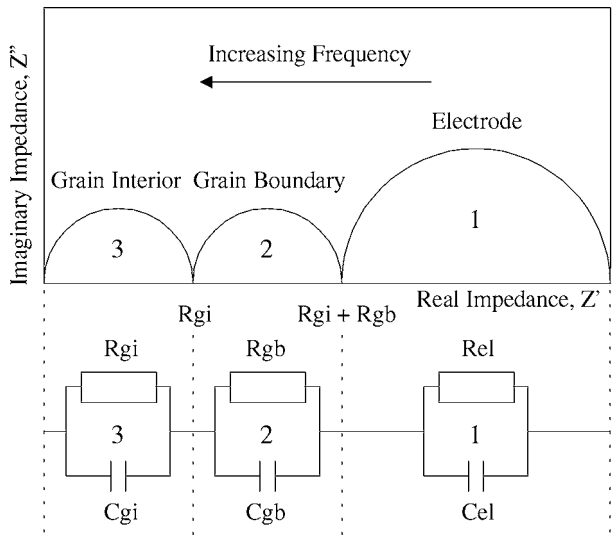

Figure 1 Idealised complex plane plot and equivalent circuit for a ceramic material.

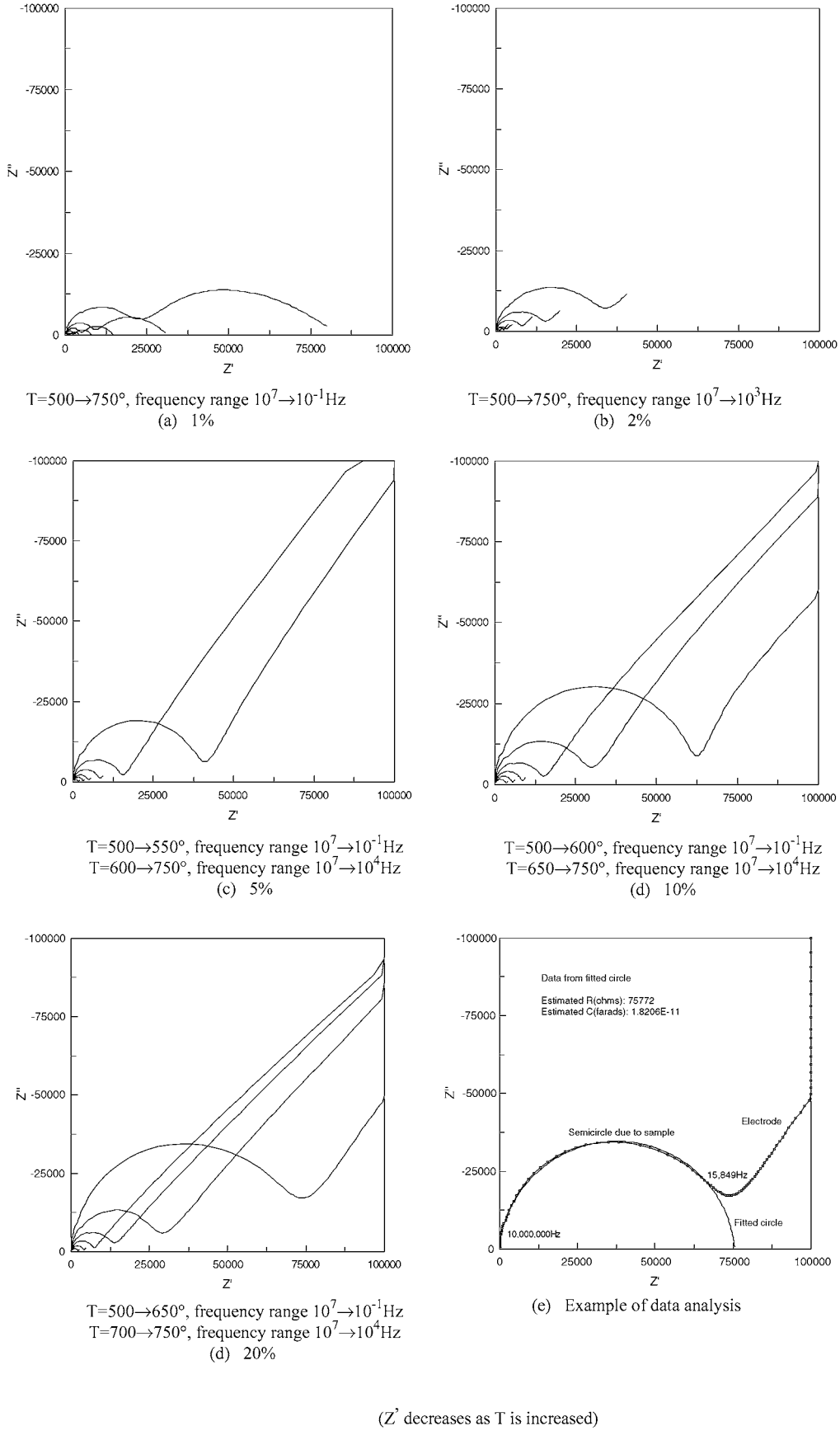

Figure 2 (a–e) Complex plane plots for composite samples.

shown in Fig. 3. The same trend, of a decrease in conductivity with addition of zirconia, is repeated over the specified temperature range. Previous research [13], albeit with higher proportions of zirconia with smaller particle sizes thus resulting in a more homogeneous distribution of zirconia within the ceria, exhibited a reduction in conductivity. This was found to be due to the formation of a solid solution, suggesting that a similar reaction may be occurring within the present composite samples.

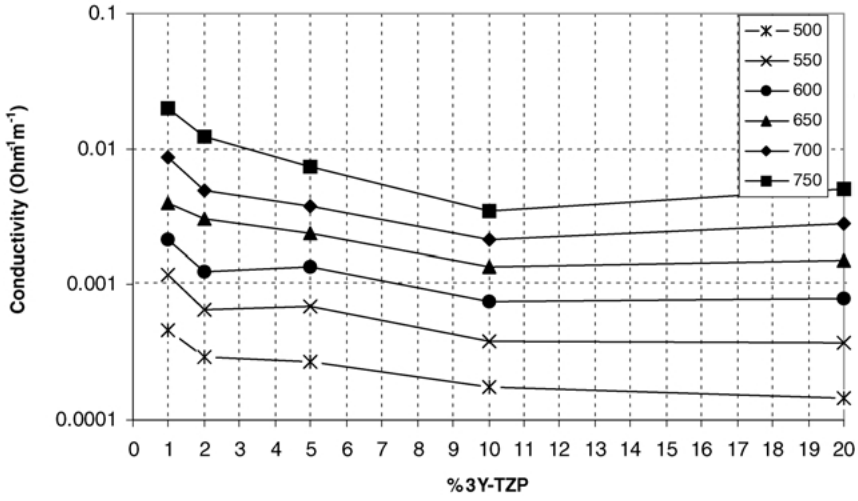

Figure 3 Conductivity versus composition for composites in the temperature range 500 to 750°C.

Values of activation energy for ionic conduction can be obtained from the Arrhenius equation described earlier. A plot of ln(conductivity $*$ T) versus $1/T$ is given in Fig. 4. Linear regression lines have been fitted to each set of data, the gradient of which are directly proportional to the activation energy for ionic conduction. Correlation coefficients, R^2, are all $\geq$0.9895 indicating a very good fit. Calculated activation energies for ionic conduction are given in Fig. 5. It is apparent that all values lie in the range 0.88–1.07 eV. These values are within the range that would be expected, considering experimental variations and errors.

X-ray diffraction patterns obtained from the sintered ceramic samples are shown in Fig. 6, with the characteristic peaks labelled. All peaks identified could be correlated with standard crystallographic data from the CeO_2, Gd_2O_3 or tetragonal-ZrO_2 patterns. This suggests that no additional compounds formed by reaction between the components, or that any impurities are present within the samples. It should be noted that all patterns have been normalised to 100, relative to the sum of the intensities of the CeO_2 (111) and ZrO_2 (111) peaks. A plot of the normalised intensity of the ZrO_2 (111) peak versus % 3Y-TZP particles is given in Fig. 7. The relationship is linear with a correlation coefficient of 0.9916, however the normalised peak intensity is not equal to the percentage of zirconia present. This is a likely consequence of differences in mass adsorption coefficient of the two oxides due to their different relative atomic masses. It should be noted that even when the proportion of zirconia within the sample is as little as 1% the zirconia (111) peak is still resolvable, suggesting that the majority of zirconia particles have remained as particles and not dissolved into the ceria to form a solid solution.

The fracture strength of the composite samples was determined using bending tests in the ball and ring configuration. A plot of fracture strength versus composition is shown in Fig. 8. Each point represents the mean fracture strength of 10 samples tested and error bars

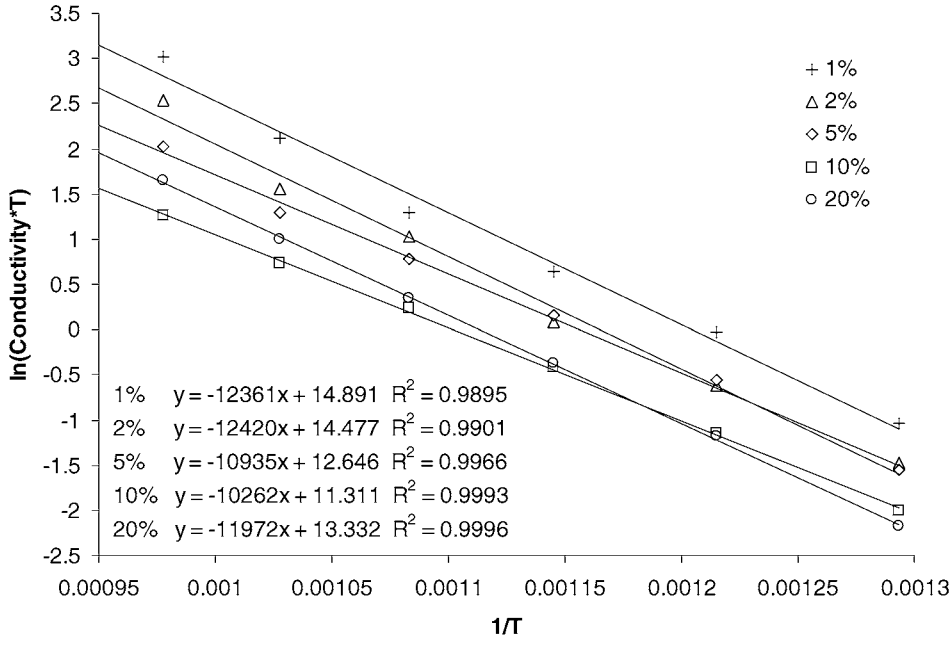

Figure 4 Arrhenius plots for experimental composites containing 1, 2, 5, 10 and 20% yttria stabilised zirconia.

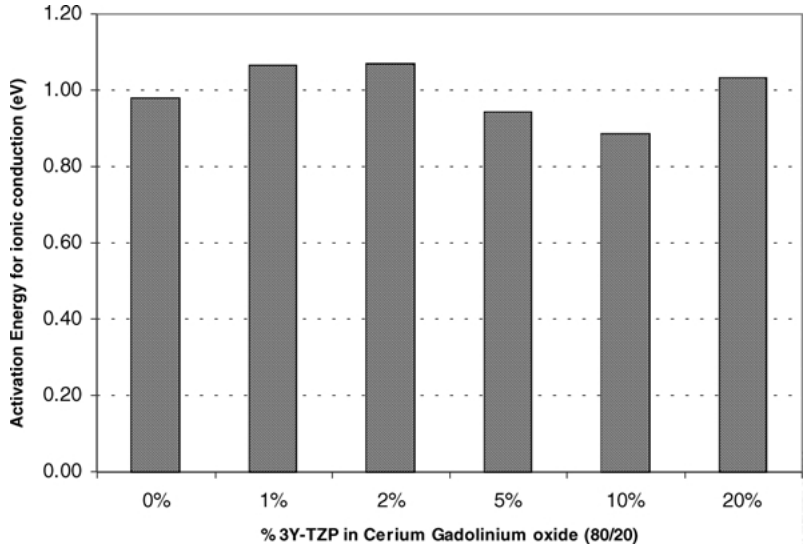

Figure 5 Activation energies for ionic conduction of experimental composites containing 1, 2, 5, 10 and 20% yttria stabilised zirconia.

Figure 6 X-ray diffraction patterns for each composite sample.

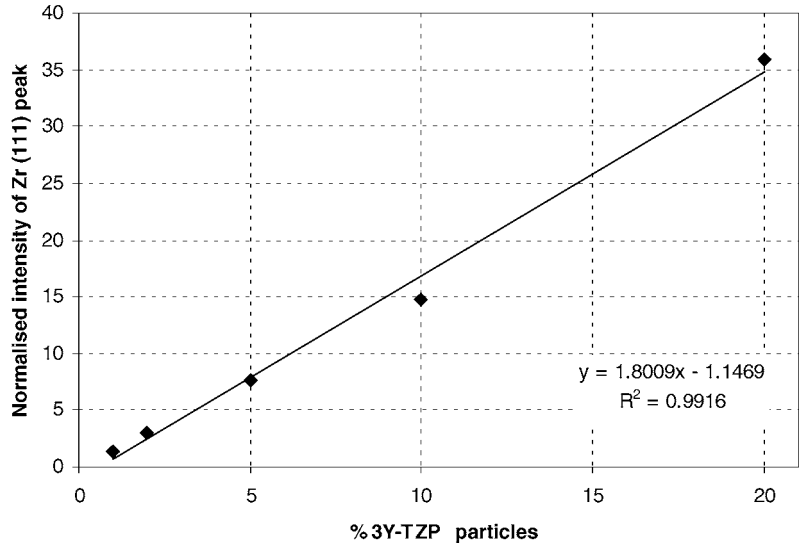

Figure 7 Normalised intensity of zirconia (111) peak versus composition.

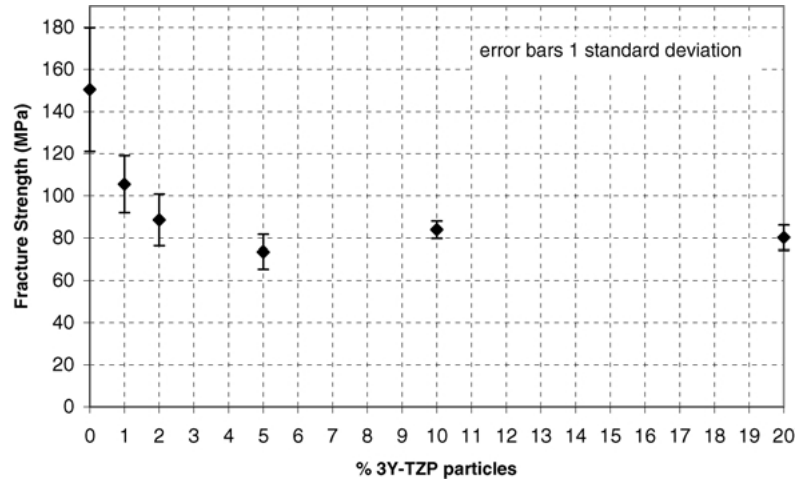

Figure 8 Fracture strength versus weight percentage zirconia particles added to sample.

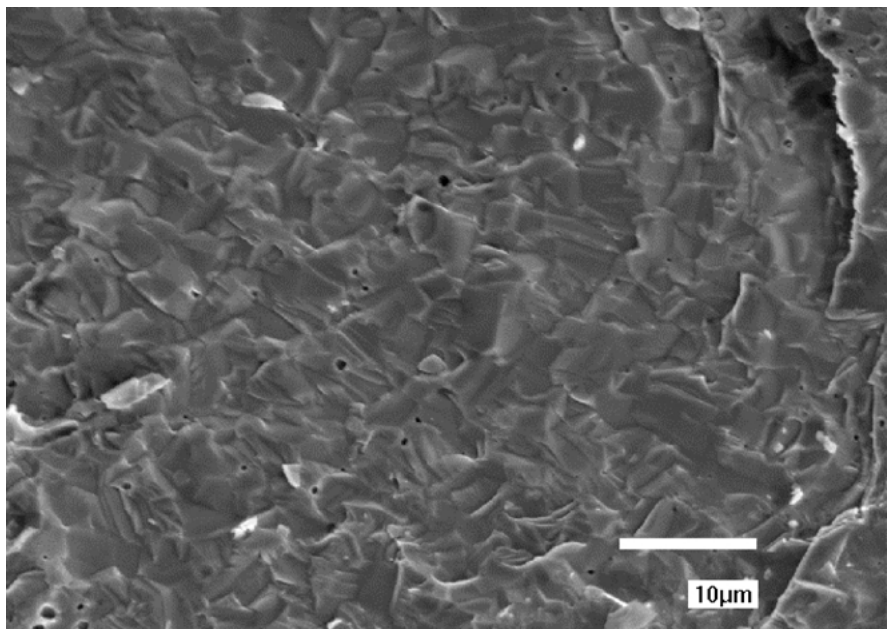

Figure 9 Fracture surface of gadolinia doped ceria composite matrix.

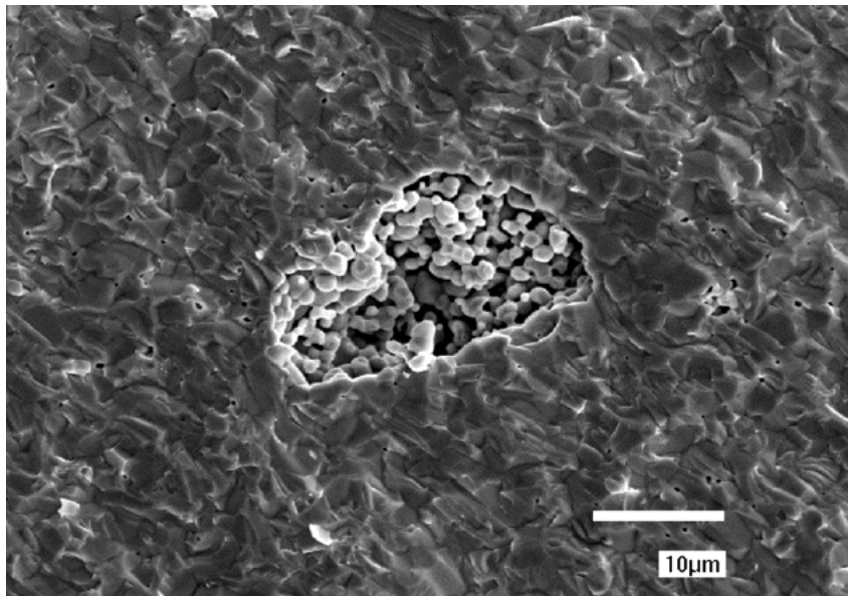

Figure 10 Fracture surface showing area of very high porosity.

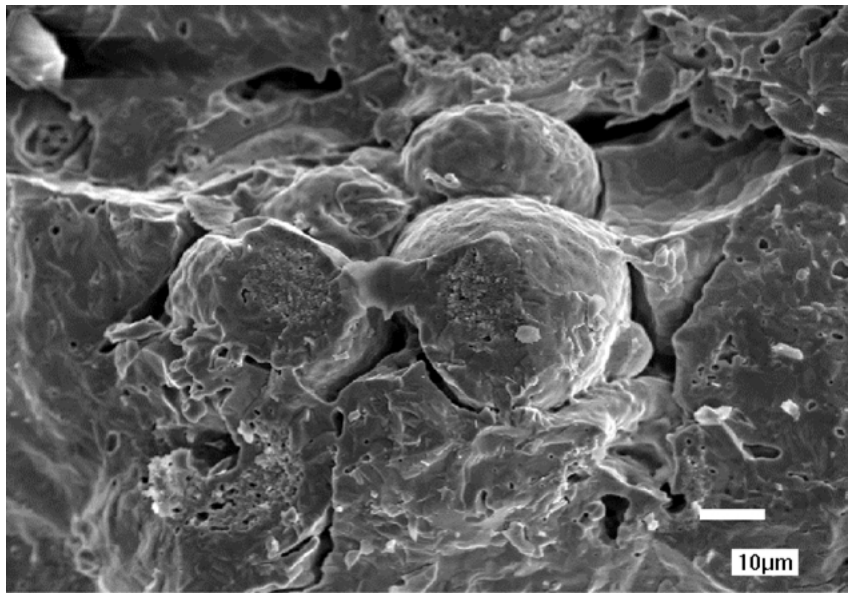

Figure 11 Fracture surface showing an intact group of agglomerated zirconia particles.

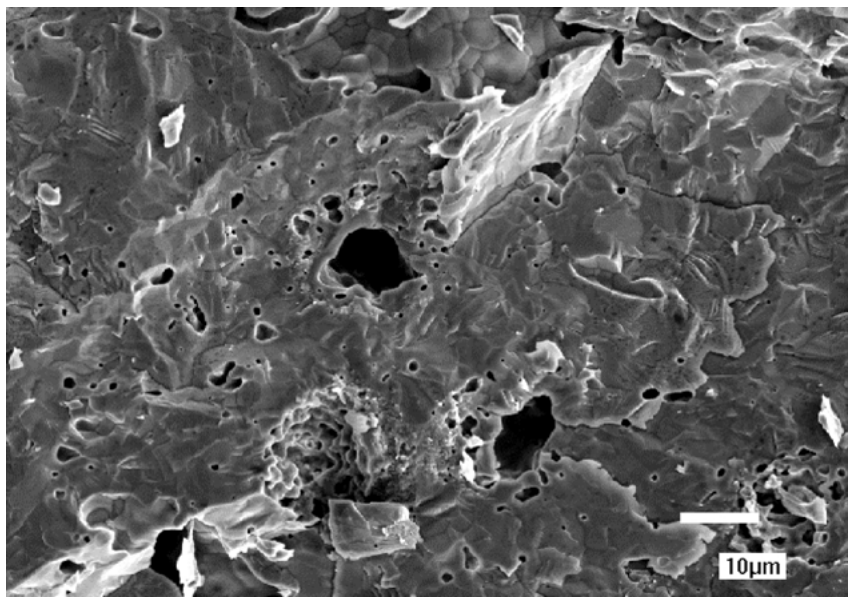

Figure 12 Fracture surface showing cross section of zirconia particle.

show 1 standard deviation. From the figure it is apparent that the addition of zirconia results in a decrease in fracture strength up to approximately 5%, after which the fracture strength remains constant. It is interesting to note that a decrease in the standard deviation also occurs with increasing zirconia content. This result suggests that the zirconia particles are acting as points of stress concentration where cracks can initiate. However, particles also have the ability to reduce the rate of crack propagation by acting as crack stoppers. This may well be a likely explanation for the plateau at zirconia concentrations above 5 wt%.

An SEM micrograph of a typical fracture surface is shown in Fig. 9. A small amount of porosity is visible distributed evenly throughout the surface. Measurements on the samples indicated porosities up to 10%. Areas of very high porosity are shown in Fig. 10, this indicates incomplete sintering and may be a result of the presence of a zirconia particle. A small agglomerate consisting of several zirconia particles, exposed by specimen fracture, is shown in Fig. 11. The majority of the particles appear to be intact and it is interesting to note the void present around each particles perimeter. Fig. 12 shows a spray dried particle fractured across its central region. The particle appears to have formed a good bond between itself and the ceria matrix. A large void is visible in the centre of the particle, this originates from when the particle was formed during spray drying. An example of the various types of porosity identified within the samples is given in Fig. 13. Porosity similar to that observed adjacent to the zirconia particles is visible, (A), in addition to green porosity, (B), originating from when the sample was in the green state. As the only difference between samples was the number of zirconia particles, the features described were present to a certain degree in all samples.

In addition to SEM a number of samples were prepared for transmission electron microscopy. TEM examination of the samples did not reveal the presence of any zirconia particles. It is highly probable that these would not have survived intact in the TEM specimens during the sample preparation procedure due to (i) the relatively large size of the zirconia particles and agglomerates in comparison to the TEM sample thickness and (ii) the high porosity and voids present around the parameter of the particles. Despite this, micrographs were obtained which show a number of interesting features within the ceria/gadolinia matrix.

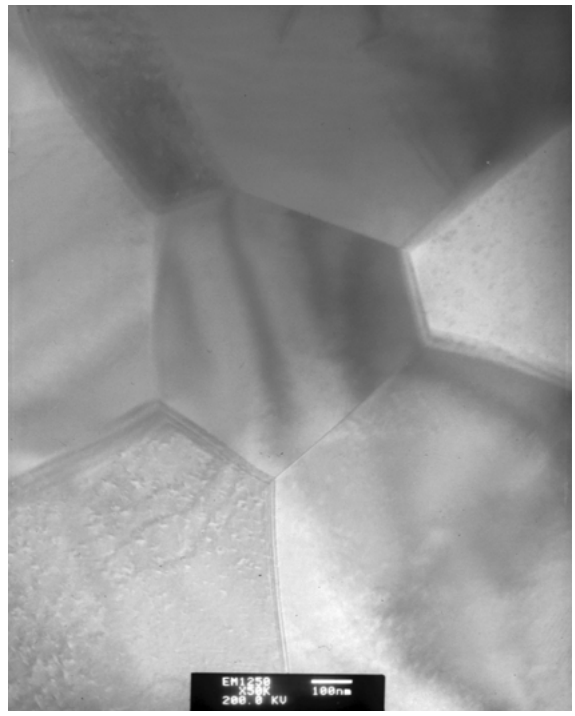

Figure 14 TEM micrograph of gadolinia doped ceria showing grain sizes and grain boundaries.

Figs 14 and 15 show a selection of uniformly sized ceria grains. No precipitates were observed within the grain boundaries, as would be expected from earlier X-ray diffraction results. A spotty effect can be seen

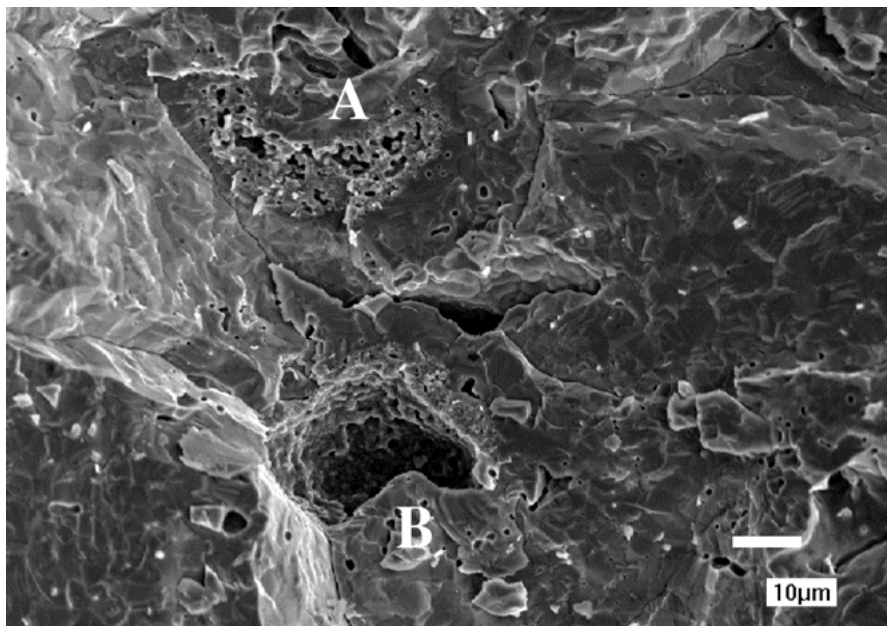

Figure 13 Fracture surface showing different types of porosity identified in sample.

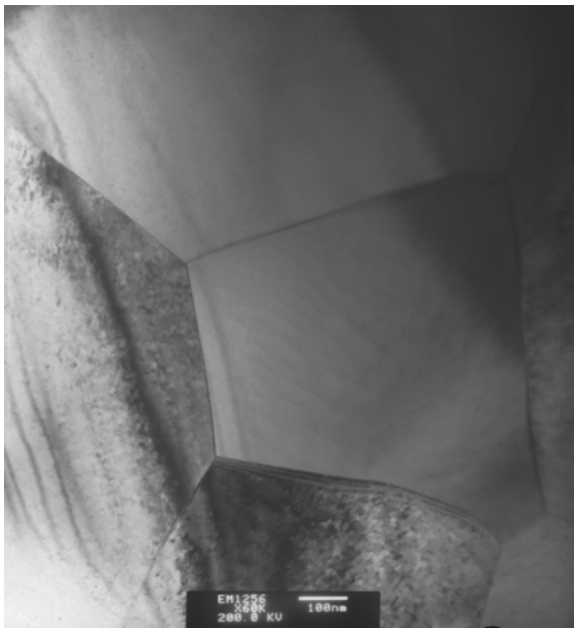

Figure 15 TEM micrograph of gadolinia doped ceria showing grain sizes and grain boundaries.

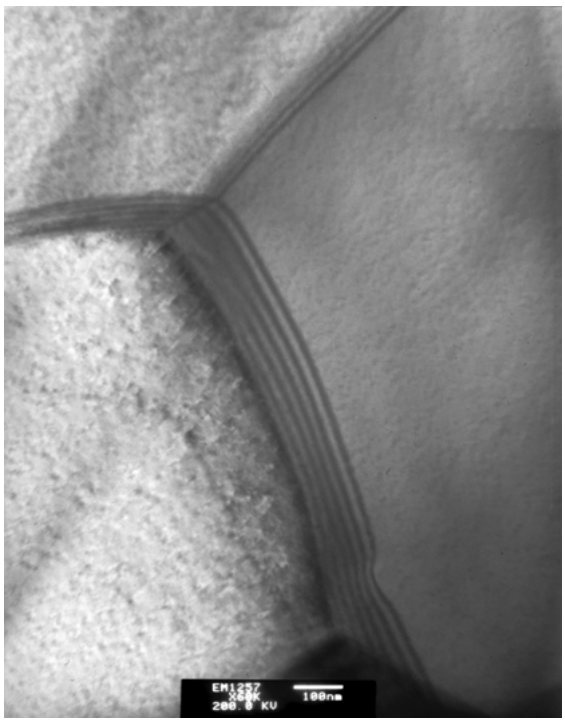

Figure 16 TEM micrograph of gadolinia doped ceria showing a number of fringes along a grain boundary, caused by diffraction of the electron beam.

on some of the grains, especially those in Fig. 15, this is likely to be a result of damage caused by ion bean thinning and may well suggest the presence of interstitial argon in the sample although this has not been verified. A high magnification micrograph of a grain boundary showing diffraction induced grain boundary thickness fringes is shown in Fig. 16. It is apparent that the grain boundaries are 'clean', that there is no crystalline second phase present and that if there is a glass phase present it is very thin. Fig. 17 shows the presence of grown in dislocations in a large grain.

Figure 17 TEM micrograph of gadolinia doped ceria showing dislocations within a grain.

4. Conclusions

This study has demonstrated that rather than increasing strength, the addition of spray dried zirconia particles to a gadolinia doped ceria matrix in fact reduces it. Examination of the composites using a SEM identified areas of high porosity and the presence of cracks around the edges of particles. It is believed that the reduction in strength is a consequence of the initiation and propagation of cracks from these areas. A reduction in conductivity with the addition of zirconia particles was also observed in results obtained from impedance spectroscopy and is consistent with the formation of a solid solution. In addition, the following general conclusions can be drawn:

1. The frequency response of the composite samples, in the temperature range of 500 to 750°C, consisted of only one semicircle on the complex plane plot, suggesting the grain interior conductivity is dominant. Examination using TEM showed clean grain boundaries with no precipitates visible.
2. Activation energies for ionic conduction did not vary significantly between samples of different composition.
3. X-ray diffraction patterns produced from sintered composite samples all contained the ZrO_2 (111) peak, even at 1 wt% ZrO_2 concentration, suggesting that the particles had undergone only limited dissolution into the doped ceria matrix. The relationship between the intensity of the ZrO_2 (111) peak on each x-ray diffraction pattern obtained, and the wt% of zirconia particles in the matrix is linear.
4. Decreases in fracture strength were observed as the proportion of zirconia in the sample increases and reaches a plateau at additions of 5 wt% or greater.

References

1. S. P. S. BADWAL and K. FOGER, *Ceramics International* **22** (1996) 257.
2. J. E. SHEMILT, H. M. WILLIAMS, M. J. EDIRISINGHE, J. R. G. EVANS and B. RALPH, *Scripta met. & mat.*, in press.
3. LARMINE DICKS, "Fuel Cell Systems Explained" (John Wiley & Sons, 2000) p. 166.

4. J. P. P. HUIJSMANS, *Current Opinion in Solid State and Materials Science* **5** (2001) 317.
5. NGUYEN Q. MINH, *J. Amer. Ceram. Soc.* **76**(3) (1993) 563.
6. K. EGUCHI, T. SETOGUCHI, T. INOUE and H. ARAI, *Solid State Ionics* **52** (1992) 165.
7. KOICHI EGUCHI, *Journal of Alloys and Compounds* **250** (1997) 486.
8. B. C. H. STEELE, in "Ceramic Oxygen Ion Conductors and Their Technological Applications," edited by B. C. H. Steele (Institute of Materials, London, 1996) p. 151.
9. D. SCHNEIDER, D. GÖDICKEMEIER and L. J. GAUKLER, in "Ceramic Oxygen Ion Conductors and Their Technological Applications," edited by B. C. H. Steele (Institute of Materials, London, 1996) p. 103.
10. N. BONANOS, R. K. SLOTWINSKI, B. C. H. STEELE and E. P. BUTLER, *J. Mater. Sci. Lett.* **3** (1984) 245.
11. N. SAMMES, *et al.*, *Denki Kagaku* **64** (1996) 674.
12. H. YAHIRO, *et al.*, *J. Appl. Electrochem.* **18** (1988) 527.
13. J. LUO, R. J. BALL and R. STEVENS—Unpublished work.
14. Standard test method for biaxial flexure strength (modulus of rupture) of ceramic substratesm, ASTM Designation: F 394–78 (Reapproved 1991).
15. J. R. MACDONALD and W. B. JOHNSON, in "Fundamentals of Impedance Spectroscopy-Impedance Spectroscopy: Emphasizing Solid Materials and Systems," edited by J. R. MacDonald (John Wiley & Sons, 1987) p. 1.
16. J. E. BAUERLE, *J. Phys. Chem. Solids.* **30** (1969) 2657.
17. J. A. KILNER and R. J. BROOK, *Solid State Ionics* **6** (1982) 237.
18. P. G. BRUCE, "Solid State Electrochemistry" (Cambridge University Press, 1997).

Received 29 May
and accepted 21 November 2002